J Mater Sci (2024) 59:3087–3100

Metals & corrosion

Uncovering the generic and alloy-specific governing parameters of deformation-induced martensitic transformation in austenitic steel

Chunguang Shen[1,2,3], Wangzhong Mu[2,4], Chenchong Wang[1], Wei Xu[1,*], and Peter Hedström[2,5,*]

[1] State Key Laboratory of Rolling and Automation, Northeastern University, Shenyang 110819, Liaoning, China
[2] Department of Materials Science and Engineering, KTH Royal Institute of Technology, Brinellvägen 23, 100 44 Stockholm, Sweden
[3] Tianjin Key Laboratory of Materials Laminating Fabrication and Interface Control Technology, School of Materials Science and Engineering, Hebei University of Technology, Tianjin 300401, China
[4] Engineering Materials, Division of Materials Science, Department of Engineering Science and Mathematics, Luleå University of Technology, Luleå 97187, Sweden
[5] Ferritico, Valhallavägen 79, 114 28 Stockholm, Sweden

Received: 16 March 2023
Accepted: 27 December 2023
Published online: 12 February 2024

ABSTRACT

In this work, a hybrid modeling approach, combining machine learning (ML) and computational thermodynamics, has been applied to predict deformation-induced martensitic transformation (DIMT) and explore the generic and alloy-specific parameters governing DIMT in austenitic steels. The DIMT model was established based on the ensemble ML algorithms and a comprehensive set of physical variables. The developed model is highly generalizable as validated on unseen alloys. The generic governing parameters of DIMT are in good agreement with previous studies in the literature. However, the evaluated alloy-specific governing parameters reveal large differences between grades, e.g., 204 series of austenitic stainless steels has a quite balanced correlation between strain, stress, temperature, and DIMT, while the 301 series has much stronger correlation between stress and DIMT. The findings in the current study emphasize the importance that a general DIMT model for steels should include both stress and strain, as well as other governing parameters, since DIMT can be both stress-assisted and strain-induced transformation, and often the effect of applied mechanical driving force and the formation of new nucleation sites interact.

Handling Editor: Megumi Kawasaki.

Address correspondence to E-mail: xuwei@ral.neu.edu.cn; pheds@kth.se

https://doi.org/10.1007/s10853-023-09325-2

GRAPHICAL ABSTRACT

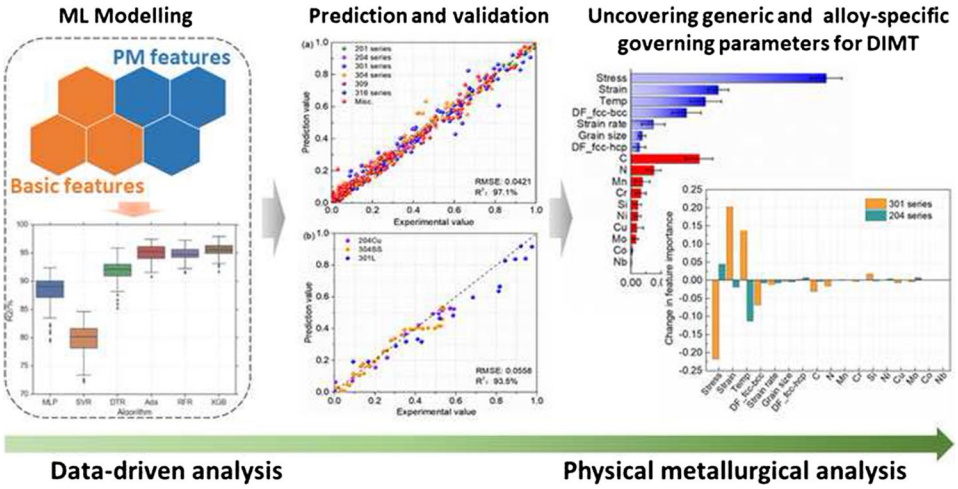

Introduction

Current development of advanced steels makes frequent use of the austenite phase and the transformation-induced plasticity (TRIP) effect to improve strain hardening, ductility, and toughness. The TRIP effect originates from deformation-induced martensitic transformation (DIMT), where the metastable austenite (fcc) is transformed to α'- and ε-martensite during the deformation [1]. Olson and Cohen [2] suggested that DIMT can occur as either stress-assisted when the applied stress is below the yield strength of the steel or as strain-induced when the applied stress is above the yield strength and when plastic deformation precedes DIMT. It is generally believed that stress, contributing a mechanical driving force, is more important than the contribution from strain generating new potent nucleation sites [3–5]. However, it is well known that α'-martensite tends to form preferentially at nucleation sites arising due to the deformation of the austenite [6]. Moreover, the dislocations from plastic strain can also retard or prevent DIMT by hindering movement of austenite/martensite interfaces [7]. Hence, the effect of strain and stress on DIMT is complex.

In order to reveal the governing parameters, numerous studies have been performed for specific alloys. Das et al. [4] could predict DIMT using the Koistinen and Marburger equation including only stress, and Chatterjee et al. [3] investigated DIMT in TRIP steels and presented that the variation in austenite fraction can be well modeled as a function of applied stress. However, there are also many modeling studies that have also treated the DIM fraction as a function of strain [8, 9]. Considering strain-induced transformation, in this case only referring to when plastic deformation and DIMT occur simultaneously without stating the main governing parameter, the Olson-Cohen model is the most commonly applied. The original Olson-Cohen model has been developed in multiple steps to consider various physical parameters affecting DIMT such as strain rate [10], stress state [11], austenite grain size [12], and pre-existing α'-martensite [13]. These models can be used in a narrow parameter space after fitting with experimental data, but a more general model capable of predicting DIMT, where also the potential difference of governing parameters for different alloys and systems could be revealed, is lacking to date. Machine learning (ML) has been widely applied to find relations among composition/processing, microstructural features, and target properties [14, 15], also for DIMT behavior in specific systems [4, 16–18]. The above studies confirm the feasibility of applying ML methods to predict DIM fraction, but they fail to achieve satisfactory general predictions of DIMT due to insufficient number of training samples. Furthermore, in those studies little attention has been paid to physical metallurgy (PM) parameters. This

Table 1 A summary of the database used in this study. Composition is in wt.%, stress in MPa, SR (strain rate) in s^{-1}, and GS (grain size) in μm; temperature in ℃, and $DF_{fcc\text{-}bcc}$ and $DF_{fcc\text{-}hcp}$ being the driving forces for transformation from austenite to α'-martensite and ε-martensite in J/mol

Grade	201 series	204 series	301 series	304 series	309	316	Misc.
C	0.03–0.05	0.04–0.08	0.001–0.15	0.006–0.79	0.054	0.02	0–0.97
N	0.2	0.04–0.24	0.01–0.17	0–0.075	0.05	0.08	0–0.31
Cr	17.0–17.5	15.0–15.4	16.6–17.6	13.4–18.7	22.1	16.2	0–18.3
Ni	3.7	1.1–2.8	6.4–7.8	8.0–9.2	12.1	10.0	0–22.8
Mn	6.7–7.4	8.9–9.0	1.1–2.0	0.9–2.0	1.9	1.7	0–20
Mo	0.01–0.05	0–0.03	0–0.8	0–0.35	0.21	2.0	0–4.1
Si	0.28–0.32	0.40–0.44	0.43–1.50	0.18–0.62	0.32	0.5	0–3
Cu	0.05–0.23	0–1.68	0–0.25	0–0.91	0.35	0.34	0–0.12
Co	0	0–0.05	0–0.14	0–0.2	0.15	0.13	0
Nb	0	0–0.001	0–0.05	0–0.015	0.02	0	0
Strain	0.37–0.57	0–0.5	0–0.65	0–0.90	0–0.3	0–0.58	0–0.78
Stress	950–1969	0–1673	0–1715	0–2307	0–863	0–1992	0–2000
SR (10^{-4})	5–100	1.3–1300	1.0–2.0 × 10^6	1.3–10^7	1.3	0.5	0.6–10
GS	15–26	0.5–40	1.2–33	7–90	30	90	7–170
Temperature	− 80 ~ 100	25	− 173 ~ 80	− 196 ~ 80	24	− 196 ~ 27	− 196 ~ 100
$DF_{fcc\text{-}bcc}$ (10^3)	1.5–2.5	1.7–2.3	2.3–4.3	1.5–4.0	2.1	2.4–3.6	− 0.5–4.0
$DF_{fcc\text{-}hcp}$ (10^2)	− 2.0 ~ 2.5	− 2.3 ~ 3.5	− 1.8 ~ 14.6	− 3.0 ~ 13.9	8.2	4.7–11.2	− 13.4 ~ 14.1
Data size	28	366	984	691	8	23	701

also means that although some discussion of governing parameters of DIMT has been provided in previous studies [16], there is no comprehensive discussion of the governing parameters of DIMT based on all/most PM parameters using advanced statistical analysis by ML. We therefore aim to build a ML model that accounts for PM parameters, including parameters calculated from computational thermodynamics. A predictive model of DIMT is established, and we comprehensively investigate the correlation between features and DIMT for austenitic steels in general and also break this down into specific alloys to investigate if the governing parameters vary between alloy systems.

Model development

Database

The database was further developed from a prior work [19] containing 2801 original datapoints from austenitic stainless steels (ASSs), such as the 201 series, 204 series, 301 series, 304 series, 309, 316, and also other related experimental alloys (Misc.). All these steels have a fully austenitic structure prior to deformation. In order to investigate the effect of the governing parameters on DIMT, the following features were included: strain, stress, strain rate, temperature, austenite grain size, driving force for α'-martensite transformation ($DF_{fcc\text{-}bcc}$), and driving force for ε-martensite formation ($DF_{fcc\text{-}hcp}$). α'-martensite fraction was the target to be predicted. In this database, α'-martensite fraction was mainly measured by saturation magnetization and x-ray diffraction (XRD) methods and the measurement error was less than 3% [20], satisfying the establishment of a reliable ML model. The database constitution is summarized in Table 1. Strain, stress, strain rate, and temperature were directly read from the related literature. The austenite grain size was most often taken from the reported values in μm, in some cases though grain size was given as an ASTM number, which were in such case transformed to μm based on ASTM E112 [21]. In other cases, the grain size was evaluated based on the micrographs reported in literature. Finally, in a few cases no grain size or microstructure information was provided in the original report, and in those cases the average value of the grain size in the database was used. Driving forces for both α'-martensite and ε-martensite were calculated by Thermo-Calc® software 2021b [22] using TCFE11 database [23]. The reason to include also ε-martensite is that DIMT is related to the stacking fault energy (SFE) which relates to $DF_{fcc\text{-}hcp}$ [2]:

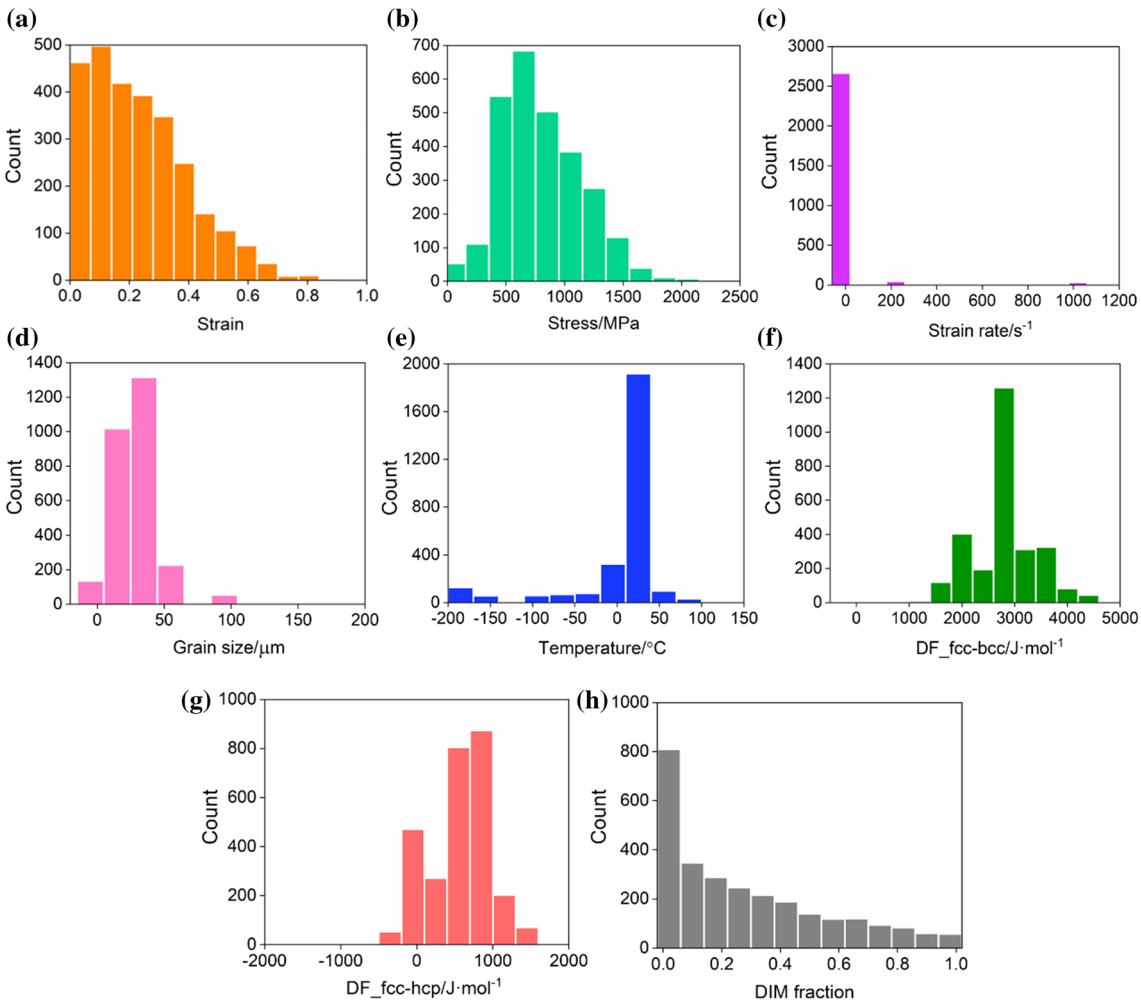

Figure 1 Statistical distribution of PM features and the output.

$$\mathrm{SFE} = 2\rho\left(\Delta G^{\gamma\to\varepsilon} + E^{\mathrm{strain}}\right) + 2^{\gamma/\varepsilon} \quad (1)$$

where ρ is atom density in a close packed plane in moles per unit area; $\Delta G^{\gamma\to\varepsilon}$ is the free energy for transformation from austenite to ε-martensite, which is equal to the negative value of $\mathrm{DF}_{\mathrm{fcc\text{-}hcp}}$. E^{strain} is the strain energy for the transformation from austenite to ε-martensite and $\sigma^{\gamma/\varepsilon}$ is the interfacial energy of the γ and ε phase boundary. E^{strain} is generally neglected in austenitic steel and the parameters ρ and $\sigma^{\gamma/\varepsilon}$ can be assumed to be constant [24]. The constitution of the PM parameters and the output in the database is shown in Fig. 1.

ML modeling

In the present work, a train–test split approach was applied where the dataset was randomly separated into a training dataset (80% of the data) and a test dataset (20% of the data). Normalization was applied to eliminate the difference in the numerical range among different input features, and the inputs are scaled to the range from 0 to 1. Based on the previous modeling results, it is found that the prediction of the trained ML model fluctuates for different partitions of the training and test sets; hence, multiple hold-out datasets were used to reliably evaluate the performance of the model [25]. The dataset was randomly divided into training and testing sets to develop 100 ML models, and model evaluation was performed by the squared correlation coefficient (R^2), mean absolute error (MAE), and root mean square error (RMSE).

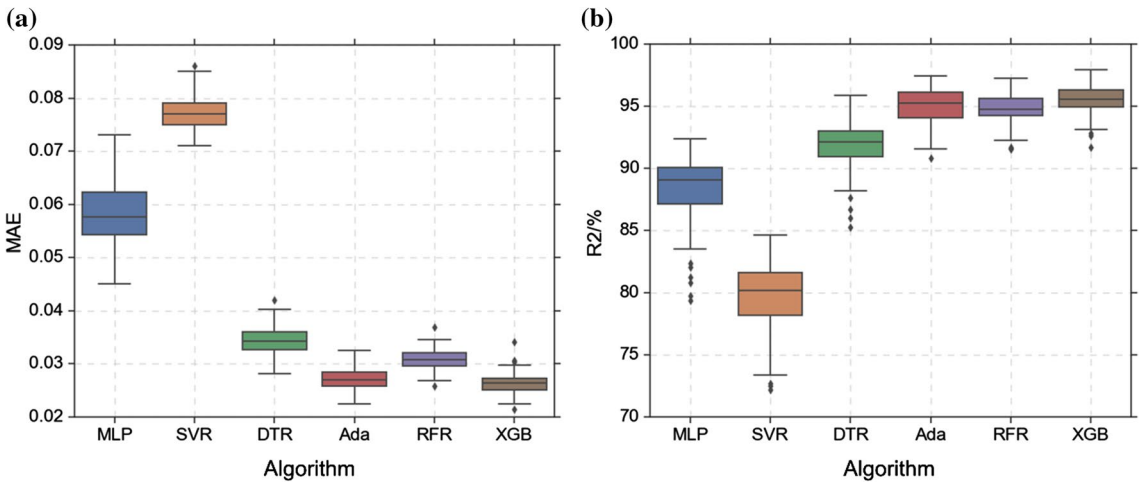

Figure 2 Prediction accuracy for different algorithms using multiple hold-out datasets and statistical error representations **a** MAE and **b** R^2.

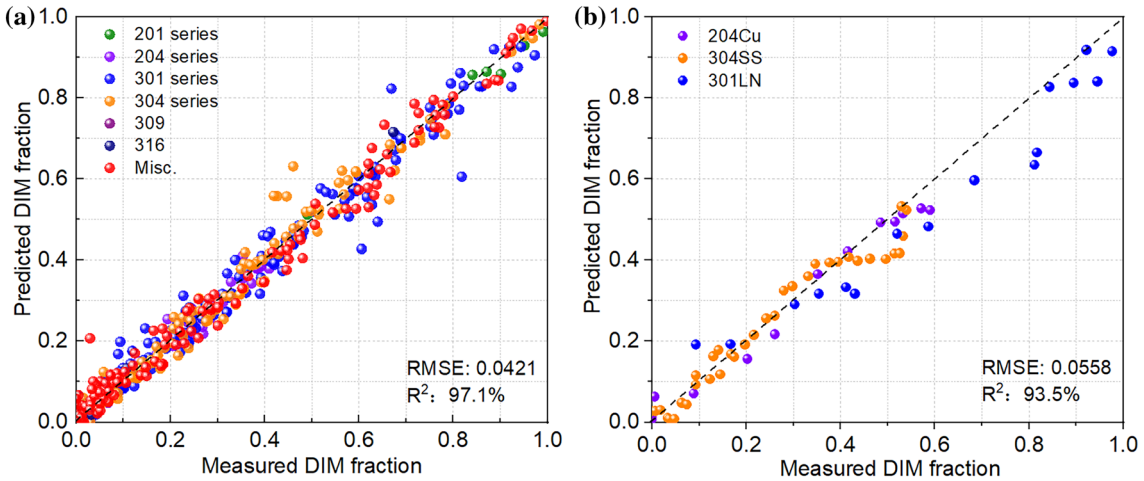

Figure 3 Experimental values vs. predicted values from the XGBoost method: **a** testing dataset; **b** unseen validation dataset.

Six ML algorithms were applied to build the correlation between input features and the DIM fraction: (1) multilayer perceptron (MLP), a kind of artificial neural network, consisting of the neuron layers and the neuron clusters in each layer, which has been widely used to address material science challenges [26]; (2) support vector regression (SVR), a statistical learning regression algorithm based on structural risk minimization principle [27], suitable to develop models in the case of the small amount of samples; (3) decision tree regression (DTR), it belongs to the nonparametric models of supervised learning used for regression analysis, which originates from a binary tree that splits into more nodes to develop a decision tree [27]; (4) ensemble learning regression, including random forest regression (RFR), Adaboost (Ada), and XGBoost (XGB), a sort of multi-regression system, which integrates the multiple learners to

Table 2 RMSE values of testing set for each grade

Grade	201 series	204 series	301 series	304 series	309	316	Misc.
RMSE	0.042	0.024	0.044	0.036	0.005	0.029	0.052

complete the modeling [28]. The grid search technique is applied to optimize the hyper-parameters of each ML models, and the optimal hyper-parameter range and key hyper-parameters of 100 models for each ML algorithm are shown below: (1) MLP (activation = relu, solver = lbfgs, size of first hidden layer: 30, size of second hidden layer: 20); (2) SVR (penalty parameter *C*: 45–49, kernel function = RBF); (3) DTR (maximum depth of tree: 42–71); (4) RFR (number of estimators: 58–94); (5) Ada (number of estimators: 66–85, base estimator: DTR); (6) XGB (number of estimators: 33–42, learning rate = 0.1). The modeling implementation was conducted using Python and the Scikit-learn library. The prediction results of the testing set are shown in Fig. 2. It can be seen that the ensemble methods have better prediction accuracy than MLP, SVR, and DTR algorithms, which is consistent with the previous work [19]. Among the ensemble methods, random forest regression (RFR) obtains the largest MAE value, while Adaboost (Ada) and XGBoost (XGB) achieve similar accuracy in both MAE and R^2 values. Finally, XGBoost was selected as the final algorithm due to its slightly better performance.

Results and discussion

Prediction results

For the training dataset, the values of RMSE and R^2 are 0.025 and 99.3%, which indicates that the trained ML model has fully learned the "knowledge" from the training data. With respect to the testing set as shown in Fig. 3a, most data points lie on or close to the straight line with a slope of 1, indicating that the prediction results are in excellent agreement with the actual values for all kinds of grades. The RMSE and R^2 values of the whole testing dataset are 0.042 and 97.1%. Additionally, 479 of 541 testing data entries have the absolute errors between experimental and predicted values within 0.05, and no large deviations occur anywhere in the whole range of data, indicating that it has a good performance. The RMSE values for each grade are listed in Table 2. In order to further investigate the applicability, the trained model was applied for predictions on an unseen validation set containing alloys with other compositions or deformation conditions; the results are shown in Fig. 3b. For 204Cu, the validation alloy with new grain size (16.4 μm) and strain rate (3×10^{-4} s^{-1}) was collected from Ref [29], and it has a higher DIM fraction compared to other 204Cu alloy (0.5–18 μm of grain size, 5×10^{-4} s^{-1} of strain rate) in the training set [30]. The 304SS validation alloy [31] with the new composition and a lower strain rate of 3×10^{-3} s^{-1} also has an obvious difference in DIMT behavior from 304SS alloy with strain rate of 3×10^{-1} s^{-1} and other alloys belonging to 304 series. Moreover, 301LN validation alloy [32] was deformed at a different strain rate compared to the other 301 grades. However, as illustrated in Fig. 3b, the trained model is capable of accurately predicting the DIM fraction for all of the validation cases (RMSE: 0.0558, R^2: 93.5%), showing the excellent generalizability.

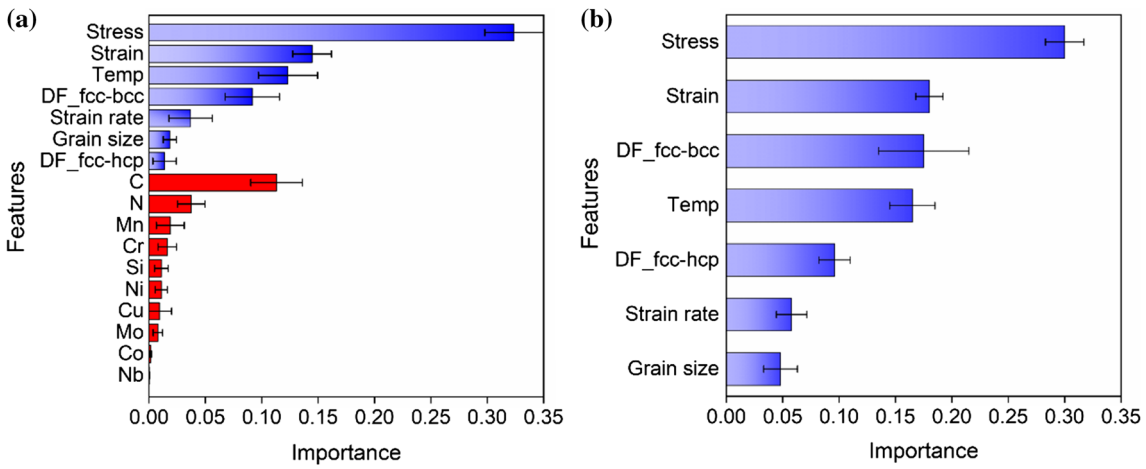

Figure 4 Feature importance analysis from ML models trained using **a** all the involved features and **b** only the PM features.

In this work, the ML method was applied to predict the DIM fraction in a very complex dataset containing a range of austenitic steel grades. However, the prediction accuracy is close to the previous studies that have only focused on one kind of austenitic stainless steels, such as AISI 304 [18] and AISI 301 [17]. Furthermore, compared to the work of Das et al. [16], the current dataset has a wider composition range and obtains a slight improvement in terms of R^2 value, i.e., 93.5% (present work) versus 88.3–95.6% (Das et al. [16]). Finally, the present prediction results are basically consistent with Ref. [19], but the amount of samples used in the current modeling process (2801 data points) is much less than in the previous study where synthetic data points were generated through physical modeling (16,500 data points).

Importance of features for DIMT

After establishing the predictive model, we investigate the correlation between composition, PM features, and DIMT based on feature importance analysis for the ML models. According to the modeling results, the feature importance was slightly different for the above four ensemble algorithms, and since each algorithm had an excellent goodness of fitting, we use the average results of feature importance from the algorithms (i.e., Ada, RFR, XGB and DTR) as final feature importance, see Fig. 4a. With respect to composition, carbon and nitrogen have the strongest correlation with DIMT and thereafter Mn, Cr, Si. For PM features, the highest importance is related to stress and thereafter strain and temperature. Strain rate and austenite grain size show relatively low importance for DIMT compared with other features.

Effect of strain and stress

The main governing parameter of DIMT behavior, i.e., stress or strain, have been discussed for a long time. Stress contributes to provide the mechanical driving force to overcome the barrier of transformation. Strain contributes to generate defects, e.g., shear bands and twins, to obtain new and potent nucleation sites for martensite and lower the driving force required for formation. Revealing these different governing mechanisms and which is the dominant feature relating to DIMT is important for deep understanding of the physical mechanisms. As illustrated in Fig. 4a, the present model shows that stress has a higher correlation than strain, and this result can be interpreted based on experiments and theoretical calculations. The study of Geijselaers et al. [33] presented that the variation in DIMT rate is basically proportional to the change of mechanical DF based on the plane-stress biaxial test, indicating that the DIMT is mainly a stress-driven process. In most modeling studies, the DIMT formation has been considered as a function of plastic strain [8]. But I. Tamura [34] argued that the transformation should be established based on the applied stress rather than strain according to the fact that martensite transformation is activated mainly by the shear stress. Also, he proposed a stress-driven model elaborating on the concept of mechanical driving force. Das et al. [4] only applied the stress value to reliably predict the DIM fraction based on the Koistinen and Marburger equation, without the consideration of strain. It is noted that the calculation result overestimated the martensite fraction, which further demonstrated that strain contributed very little to DIMT behavior. Chatterjee et al. [3] investigated the dominant mechanism of DIMT in TRIP-assisted steels and presented that the variation in austenite fraction can be well described by a function of applied stress by considering the mechanical DF, not strain. Moreover, their theoretical framework showed that the critical strain to transform austenite to martensite varies as a function of the composition and the temperature, but its contribution is certainly lower than the stress contribution [35]. In addition to kinetics, α'-martensite texture can also be predicted using the variant selection based on the mechanical DF provided by the applied stress, without the consideration of any intermediate transformation [36]. Moreover, the data-driven analysis supports the present result as well. Das et al. [16] used the ML method to analyze the quantitative correlation between these two factors and DIM fraction and presented that stress has a stronger effect than strain.

Effect of chemical elements

In general, the chemical composition controls the DIMT by affecting the chemical DF and SFE [37]. The two interstitial elements, i.e., C and N, show a very high correlation with DIMT. The addition of these elements can improve both the mechanical stability of austenite against martensite transformation by

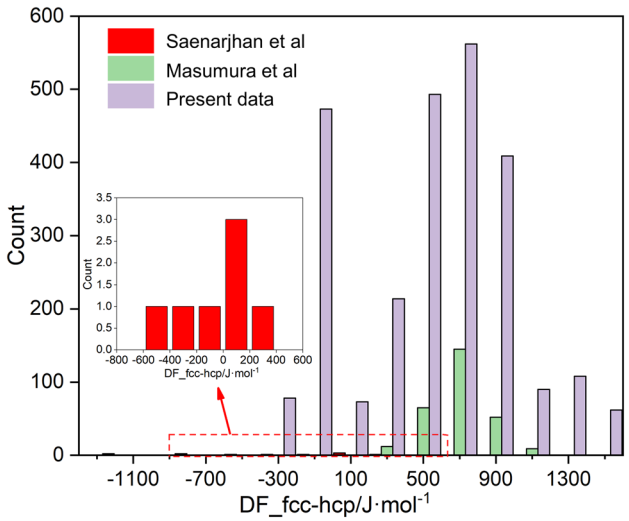

Figure 5 $DF_{fcc\text{-}hcp}$ distributions of dataset and literature [43, 45].

reducing the chemical DF [38, 39]. Moreover, C addition results in an obvious SFE increase for austenite [40], but the effect of N addition on SFE is uncertain; it depends on the host alloy composition [40–42]. Furthermore, it is still controversial whether C or N is more important for DIMT [43–45]. Masumura et al. [43] reported that the mechanical stability of C-added steel is higher than that of N-added steel based on 304 grade, and microstructure characterization shows that twins and ε-martensite are preferentially formed in C-added steel, contributing to suppress the growth of α'-martensite. But N-added steel with a higher SFE preferentially develops dislocation cell structures. Saenarjhan et al. [45] presented an opposite result based on an experimental steel (15Cr-15Mn-4Ni based ASSs), in which N-added steel obtains a higher mechanical stability because N-added steel also can develop ε-martensite, contributing to suppress transformation. In austenitic stainless steel, the SFE level determined by $DF_{fcc\text{-}hcp}$ highly affects the type of deformation microstructure. The $DF_{fcc\text{-}hcp}$ distribution of the present dataset and the data in Refs. [43, 45] is plotted in Fig. 5. It is clearly seen that most samples in the dataset have relatively large $DF_{fcc\text{-}hcp}$ values, which is similar to the distribution from the work of Matsumura et al., i.e., C obtains a higher importance than N. Apart from C and N elements, other elements show a relatively low importance. Moreover, the two DF variables that strongly affect the austenite stability also obtain low correlation. These results could be attributed to the overlap of the inputs because the two DF variables are determined by the steel composition. In order to show the true correlation to the DFs, another ML model was trained without the compositional input, and the new feature importance is plotted in Fig. 4b. It is seen that only the importance of the DF variables changes significantly, and other PM variables remain stable. The correlation of $DF_{fcc\text{-}hcp}$ was greatly enhanced and exceeded the importance of strain rate and grain size, and the correlation of $DF_{fcc\text{-}bcc}$ exceeds the deformation temperature and is very close to strain, showing the close relation between the two DFs and the austenite stability.

Effect of prior austenite grain size

With respect to prior austenite grain size, a general conclusion is that the increasing grain size is beneficial to increase DIMT owing to the decreasing austenite stability [46–48]. For instance, Jung et al. [47] found the starting temperature of transformation is linearly lowered by a reduction in austenite grain size in 301 and 304 grades. The experimental results of Varma et al. [46] show that martensite formation can be enhanced by using large austenite grain size in 304 and 316 grades. However, specific studies show conflicting findings. Shrinivas and co-workers reported that the volume fraction of martensite formed is basically unchanged as the grain size changes from 77 to 200 μm in 316SS [49]. Moreover, Kisko et al. [30] found an anomalous experimental result based on 204Cu grade; the steel with a ultrafine grain size of 0.5 μm had a higher transformation rate than the steels with relatively larger grain sizes of 1.5 μm, 4 μm, and 18 μm. Recently, Sohrabi et al. [50] found a transition when the prior austenite grain size is in the range of 34–90 μm. DIMT can be promoted when increasing the grain size up to the transition range, but it is suppressed at coarser grain sizes. Based on the above analysis, it is concluded that austenite grain size does not have a clear effect on DIMT and the relation can depend on the steel grade because factors such as effective SFE and nucleation sites can have different importance in different grades. Thus, a relatively low correlation was obtained for prior austenite grain size.

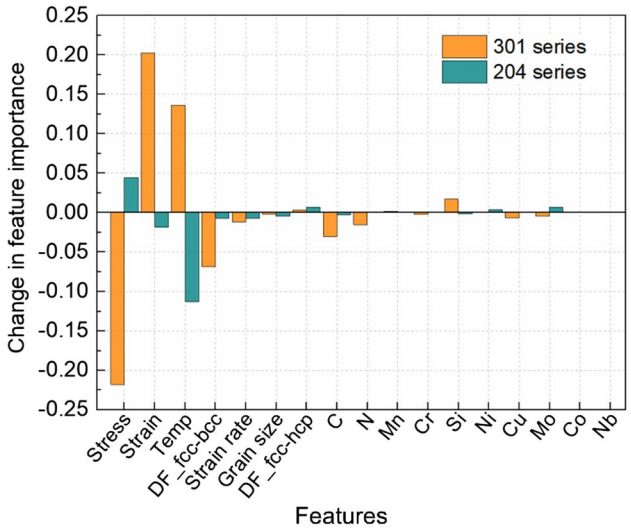

Figure 6 Change of feature importance when either the data of 204 or 301 series are removed. Positive values represent the decrease in correlation for the target grade, and negative values stand for increasing correlation.

Effect of strain rate and temperature

One of the improvements in the current database compared with our previous DIMT model [19] is including the data entries with various strain rates. The former database only focused on low strain rate ($< 0.001\ s^{-1}$). For the case of strain rate, most studies show that the increase generally suppresses the formation of DIM [51–53], which can be explained by the decrease in the chemical DF caused by the adiabatic heating and the formation of irregular shear band arrays. In contrast, the experimental results of Talonen et al. [54] show that the change of strain rate from 3×10^{-4} to $2 \times 10^{2}\ s^{-1}$ has an obvious influence, decreasing the transformation in 301 grades. But the DIM fraction does not show the obvious alteration in the 304 grades with an inherent relatively high mechanical stability. Furthermore, the high strain rate was not found to promote the DIM formation at a low strain range, contrary to the experimental observations of Hecker et al. [51]. The relatively weak correlation of strain rate and DIMT as well as some unclear effects observed in different grades in the literature causes the low feature importance of strain rate.

Additionally, the deformation temperature directly determines the chemical DF and SFE. This factor has a very clear and strong effect on the formation of DIM [55, 56], so the feature achieves a relatively high importance, larger than austenite grain size and strain rate.

Feature importance for specific steel grades

The correlation of each feature and DIMT has been generally analyzed for the whole dataset containing various grades of austenitic stainless steels in the last section, and it can be found that the correlation of some PM features varies among different steel grades. So, it is necessary to critically analyze the feature importance for the specific grades. In general, a ML model was supposed to be firstly trained by samples from the specific grades in order to obtain its importance analysis. But the sub-dataset of each steel grade does not contain enough samples and has the very narrow range of each feature, e.g., chemical composition, which increases the difficulty for training a reliable model. Instead in this work, a method is proposed to calculate the feature importance of the specific steel grade, in which samples of the target grade were removed from the dataset and a new feature importance was obtained from the new model trained by the rest of the samples. In this case, compared to feature importance of the whole dataset (Fig. 4a), a change of the importance value was attributed to the removed samples of the target grade. If the importance value of some features decreases, it indicates that these features are very important for target grade. Conversely, the increase in importance value represents a low correlation. This analysis method was applied to two series of austenitic stainless steels to investigate their respective feature importance, including 204 series (204Cu, 204 M, 204SS) and 301 series (301, 301L, 301LN), and it has been proved that 204 series has the higher austenite stability than 301 series according to the previous studies [57, 58]. Figure 6 displays the change of importance value for these selected grades. 301 series and 204 series display the totally different results. With respect to 301 series, stress greatly increases the correlation owing to the obvious reduction in importance value, and the strain and temperature become less important. This grade has the relatively low austenite stability owing to the low SFE value, e.g., $\gamma_{SFE} = 14.7\ mJ\ m^{-2}$ for 301SS [57]. The low austenite stability indicates that transformation can start in a wide temperature range with a high upper temperature limit and has a low requirement for extra chemical DF from the decrease in temperature, resulting in

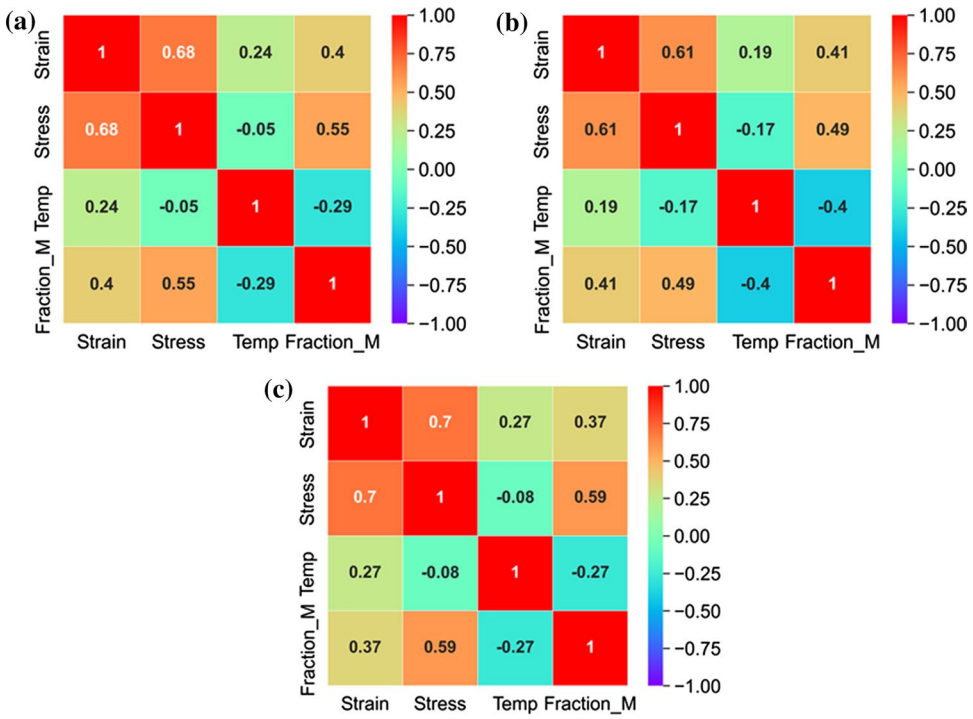

Figure 7 Pearson's correlation coefficient calculated by **a** the whole dataset, removing **b** 301 series and **c** 204 series from the dataset, respectively.

a relatively low correlation of deformation temperature. Moreover, the nucleation sites, e.g., shear bands and ε-martensite, can be easily obtained when the applied strain is very small owing to the low SFE. So, the key point governing DIMT is applied stress that provides extra mechanical DF to transform nucleation sites into α'-martensite, instead of applied strain that produces nucleation sites. With respect to 204 series, the correlation of stress and strain slightly decreases and goes up, respectively. The deformation temperature's correlation obtains an obvious increase considering the decrease in feature importance. Combining with feature importance of the whole dataset as shown in Fig. 4a, it can be seen that 204 series achieves a better balance among stress, strain, and temperature. This grade has a high austenite stability and high SFE, e.g., $\gamma_{SFE} = 16.8$ mJ m^{-2} for 204SS [57]. The high SFE represents the difficulty for forming the new nucleation sites [24], and DIMT process may be more dependent on the existing sites. In this case, the applied stress is essential to provide mechanical DF to transform the stable nucleation sites with the high activation energy. In addition, a relatively large plastic strain is also important to produce the new nucleation sites for further martensite transformation. Moreover, 204 series have a low chemical $DF_{fcc\text{-}bcc}$, which also means the extra

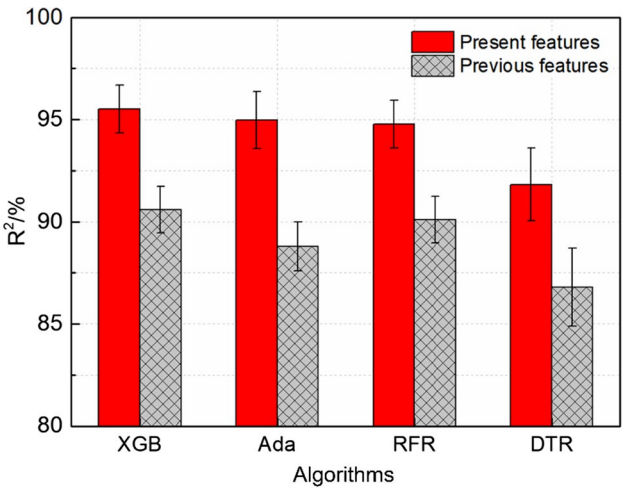

Figure 8 Prediction accuracy of ML models trained by all the features used in the present work, and only the features used in the previous work [19]. The dataset used for both models is the one presented in this work.

chemical DF from temperature reduction is important to induce transformation.

A mathematical explanation is also given to clarify the great variation in importance of strain, stress, and temperature based on the Pearson's coefficient. As shown in Fig. 7a, stress obtains a higher linear correlation than strain and temperature, showing that

stress should contribute more to the development of the ML model, which is consistent with the feature importance in Fig. 4. When removing the samples belonging to the 301 series from the dataset (Fig. 7b), the correlations of DIMT with strain and temperature increase and stress decrease (Fig. 7a), indicating that stress has a very strong correlation with α'-martensite fraction in 301 series. When removing the 204 series from the dataset (Fig. 7c), stress obtains a higher correlation, but the values of strain and temperature reduce compared to the whole dataset, also indicating that strain has a relatively higher correlation to α'-martensite transformation as compared to the 301 series.

With respect to strain rate and grain size, these factors show the decrease in importance values, indicating that they are both important for these two kinds of austenitic stainless steels. Generally, according to statistical analysis, 301 series are very different from 204 series in terms of DIMT behavior. 301 series with the low austenite stability is only highly related to applied stress, but 204 series have a higher requirement for the induction of martensite transformation, and strain, stress, and temperature all show high correlation. For the chemical composition, there are basically no obvious changes. Only a change occurs for molybdenum, and its importance reduces for 204 series because this grade contains very low level of molybdenum [29, 30]. The importance of carbon and nitrogen increases in 301 series, indicating the high correlation to DIMT.

Comparison with previous DIMT model

In the previous work of Ref. [19], a prediction model for DIMT was developed combining physical-based modeling and ML method. In order to improve the robustness of the trained ML model, a large dataset was built combining experimental data and physical modeling data using Olson-Cohen model, which provides the new methodology to combination of physical-based method and ML. The present work selects another combination method that introduces numerous related PM features into the original experimental dataset for model training, as listed in Table 1. For the prediction accuracy, the current result is very close to that of previous work, e.g., the RMSE of testing set (0.0420 vs. 0.0415), 301 series (0.0451 vs. 0.0479), and 304 series (0.0372 vs. 0.0380). But it is worth noting that the present dataset only contains 2801 samples which is significantly smaller than that of previous dataset consisting of 16,500 samples. Furthermore, in order to compare in a fair way, a new ML model was trained based on present dataset, but using features of previous work, i.e., composition, strain, and temperature. From the results in Fig. 8; it can be seen that ML models trained by present features are clearly improved than those using the previous features for each algorithm. The good performance can be interpreted by fully mining the existing data using additional PM features. In the present work, in addition to strain and temperature used in the previous work, stress, strain rate, and grain size and two kinds of DF were also included in the dataset; especially, applied stress is found to be the most important feature for DIMT prediction according to the importance analysis and previous studies [4, 16, 36] and strongly controls the DIMT process. The introduction of such crucial features aids to lower the requirement for the number of samples for training a robust model, also contributing to alleviating the small sample problem. For correlation analysis, in the previous work, strain and temperature show the very strong correlation, which is much higher than the composition. A large gap exists between PM features (strain and temperature) and composition, implying the absence of other related features. The present study introduces these missing features into modeling process and displays a whole roadmap for the correlation between various PM features and DIMT, contributing to a better understanding of PM mechanism.

Conclusions

A new predictive model for DIMT was presented in the current work based on the ensemble machine learning method combining chemical composition and various physical metallurgy features. A systematic analysis of the correlation between various factors and DIMT in general and for specific alloys was performed. The following conclusions can be drawn:

(1) The trained ML model achieved a high prediction accuracy in testing data with a R^2 value greater than 97%, and a good robustness was validated by accurately predicting the DIM fraction of unseen alloys.

(2) Feature importance analysis shows that for austenitic steels in general the most important physical metallurgy feature is stress and thereafter strain and temperature. However, the most important features vary for specific alloy grades. For example, applied stress strongly affects the DIMT behavior of 301 series, while for the 204 series, there is a stronger balance of the correlations among strain, stress, and temperature. This is due to the general higher austenite stability of the 204 series.
(3) Comparing to the authors' previous DIMT model, the introduction of new physical metallurgy features in this study assists the development of a robust model with lower requirements on dataset size. It further helps to give a comprehensive view of the correlation between DIMT and the governing physical parameters.

Acknowledgements

EIT Raw Material project ENDUREIT (Project No. 18317) is acknowledged by W.M. and P.H. for the financial support. C. S. would like to acknowledge the support from the China Scholarship Council (CSC No. No.202006080092).

Funding

Open access funding provided by Royal Institute of Technology.

Data availability

The raw/processed data required to reproduce these findings cannot be shared at this time as the data also form part of an ongoing study.

Declarations

Conflict of interest The authors declare that they have no known competing financial interests or personal relationships that could have appeared to influence the work reported in this paper.

References

[1] Injeti VSY, Li ZC, Yu B, Misra RDK, Cai ZH, Ding H (2018) Macro to nanoscale deformation of transformation-induced plasticity steels: impact of aluminum on the microstructure and deformation behavior. J Mater Sci Technol 34:745–755
[2] Olson GB, Cohen M (1976) A general mechanism of martensitic nucleation: part I. General concepts and the FCC → HCP transformation. Metall Trans A 7:1897–1904
[3] Chatterjee S, Bhadeshia HKDH (2007) Transformation induced plasticity assisted steels: stress or strain affected martensitic transformation? Mater Sci Technol 23:1101–1104
[4] Das A, Chakraborti PC, Tarafder S, Bhadeshia HKDH (2011) Analysis of deformation induced martensitic transformation in stainless steels. Mater Sci Technol 27:366–370
[5] Perdahcıoğlu ES, Geijselaers HJM, Groen M (2008) Influence of plastic strain on deformation-induced martensitic transformations. Scr Mater 58:947–950
[6] Tian Y, Gorbatov OI, Borgenstam A, Ruban AV, Hedström P (2017) Deformation microstructure and deformation-induced martensite in austenitic Fe–Cr–Ni alloys depending on stacking fault energy. Metall Mater Trans A 48:1–7
[7] Eres-Castellanos A, Caballero FG, Garcia-Mateo C (2020) Stress or strain induced martensitic and bainitic transformations during ausforming processes. Acta Mater 189:60–72

[8] Angel T (1954) Formation of martensite in austenitic stainless steels. J Iron Steel Inst 177:165–174
[9] Ludwigson DC, Berger JA (1969) Plastic behaviour of metastable austenitic stainless steels. J Iron Steel Inst 207:63–69
[10] Tomita Y, Iwamoto T (1995) Constitutive modeling of trip steel and its application to the improvement of mechanical properties. Int J Mech Sci 37:1295–1305
[11] Stringfellow RG, Parks DM, Olson GB (1992) A constitutive model for transformation plasticity accompanying strain-induced martensitic transformations in metastable austenitic steels. Acta Metall Mater 40:1703–1716
[12] Iwamoto T, Tsuta T (2000) Computational simulation of the dependence of the austenitic grain size on the deformation behavior of TRIP steels. Int J Plast 16:791–804
[13] Zheng C, Jiang H, Hao X, Ye J, Li L, Li D (2019) Tailoring mechanical behavior of a fine-grained metastable austenitic stainless steel by pre-straining. Mater Sci Eng A 746:332–340
[14] Ramprasad R, Batra R, Pilania G, Mannodi-Kanakkithodi A, Kim C (2017) Machine learning in materials informatics: recent applications and prospects, npj Comput. Mater 3:54
[15] Raccuglia P, Elbert KC, Adler PDF, Falk C, Wenny MB, Mollo A, Zeller M, Friedler SA, Schrier J, Norquist AJ (2016) Machine-learning-assisted materials discovery using failed experiments. Nature 533:73–76
[16] Das A, Tarafder S, Chakraborti PC (2011) Estimation of deformation induced martensite in austenitic stainless steels. Mater Sci Eng A 529:9–20
[17] Mirzadeh H, Najafizadeh A (2008) Correlation between processing parameters and strain-induced martensitic transformation in cold worked AISI 301 stainless steel. Mater Charact 59:1650–1654
[18] Mirzadeh H, Najafizadeh A (2009) ANN modeling of strain-induced martensite and its applications in metastable austenitic stainless steels. J Alloy Compd 476:352–355
[19] Mu W, Rahaman M, Rios FL, Odqvist J, Hedström P (2021) Predicting strain-induced martensite in austenitic steels by combining physical modelling and machine learning. Mater Des 197:109199
[20] Shirdel M, Mirzadeh H, Parsa MH (2015) Nano/ultrafine grained austenitic stainless steel through the formation and reversion of deformation-induced martensite: mechanisms, microstructures, mechanical properties, and TRIP effect. Mater Charact 103:150–161
[21] A. International, ASTM E112-13 (2013) Standard test methods for determining average grain size, ASTM International, West Conshohocken
[22] Andersson JO, Helander T, Höglund L, Shi P, Sundman B (2002) Thermo-Calc & DICTRA, computational tools for materials science. Calphad 26:273–312
[23] TCFE11: TCS Steels/Fe-Alloys Database Version 9.0 (2021) Thermo-Calc Software AB, Sweden
[24] Wang X, Xiong W (2020) Stacking fault energy prediction for austenitic steels: thermodynamic modeling versus machine learning. Sci Technol Adv Mater 21:626–634
[25] Shen C, Wang C, Wei X, Li Y, van der Zwaag S, Xu W (2019) Physical metallurgy-guided machine learning and artificial intelligent design of ultrahigh-strength stainless steel. Acta Mater 179:201–214
[26] Sumayli A (2023) Development of advanced machine learning models for optimization of methyl ester biofuel production from papaya oil: Gaussian process regression (GPR), multilayer perceptron (MLP), and K-nearest neighbor (KNN) regression models. Arab J Chem 16:104833
[27] Balogun A-L, Tella A (2022) Modelling and investigating the impacts of climatic variables on ozone concentration in Malaysia using correlation analysis with random forest, decision tree regression, linear regression, and support vector regression. Chemosphere 299:134250
[28] Liu R, Liu Y, Duan J, Hou F, Wang L, Zhang X, Li G (2022) Ensemble learning directed classification and regression of hydrocarbon fuels. Fuel 324:124520
[29] Papul S (2015) Delayed cracking of metastable low-nickel austenitic stainless steels. Department of Engineering Design and Production Engineering Materials, Aalto University, Espoo
[30] Kisko A, Misra RDK, Talonen J, Karjalainen LP (2013) The influence of grain size on the strain-induced martensite formation in tensile straining of an austenitic 15Cr–9Mn–Ni–Cu stainless steel. Mater Sci Eng A 578:408–416
[31] Shen YF, Li XX, Sun X, Wang YD, Zuo L (2012) Twinning and martensite in a 304 austenitic stainless steel. Mater Sci Eng A 552:514–522
[32] Petein A (2006) On the interactions between strain-induced phase transformations and mechanical properties in Mn–Si–Al steels and Ni–Cr austenitic stainless steels. Université Catholique de Louvain, Belgium
[33] Geijselaers HJM, Perdahcıoğlu ES (2009) Mechanically induced martensitic transformation as a stress-driven process. Scr Mater 60:29–31
[34] Tamura I (1982) Deformation-induced martensitic transformation and transformation-induced plasticity in steels. Met Sci 16:245–253
[35] Chatterjee S, Wang HS, Yang JR, Bhadeshia HKDH (2006) Mechanical stabilisation of austenite. Mater Sci Technol 22:641–644

[36] Kundu S, Bhadeshia HKDH (2006) Transformation texture in deformed stainless steel. Scr Mater 55:779–781
[37] Sohrabi MJ, Naghizadeh M, Mirzadeh H (2020) Deformation-induced martensite in austenitic stainless steels: a review. Arch Civ Mech Eng 20:124
[38] Gavriljuk VG (2006) Austenite and martensite in nitrogen-, carbon- and hydrogen-containing iron alloys: similarities and differences. Mater Sci Eng A 438–440:75–79
[39] Behjati P, Kermanpur A, Najafizadeh A (2013) Influence of nitrogen alloying on properties of Fe318Cr312Mn3XN austenitic stainless steels. Mater Sci Eng A 588:43–48
[40] Lee T-H, Shin E, Oh C-S, Ha H-Y, Kim S-J (2010) Correlation between stacking fault energy and deformation microstructure in high-interstitial-alloyed austenitic steels. Acta Mater 58:3173–3186
[41] Stoltz RE, Vander Sande JB (1980) The effect of nitrogen on stacking fault energy of Fe-Ni-Cr-Mn steels. Metall Trans A 11:1033–1037
[42] Soussan A, Degallaix S, Magnin T (1991) Work-hardening behaviour of nitrogen-alloyed austenitic stainless steels. Mater Sci Eng A 142:169–176
[43] Masumura T, Nakada N, Tsuchiyama T, Takaki S, Koyano T, Adachi K (2015) The difference in thermal and mechanical stabilities of austenite between carbon- and nitrogen-added metastable austenitic stainless steels. Acta Mater 84:330–338
[44] Wendler M, Hauser M, Fabrichnaya O, Krüger L, Weiß A, Mola J (2015) Thermal and deformation-induced phase transformation behavior of Fe–15Cr–3Mn–3Ni–0.1N–(0.05–0.25)C austenitic and austenitic–martensitic cast stainless steels. Mater Sci Eng A 645:28–39
[45] Saenarjhan N, Kang J-H, Kim S-J (2019) Effects of carbon and nitrogen on austenite stability and tensile deformation behavior of 15Cr-15Mn-4Ni based austenitic stainless steels. Mater Sci Eng A 742:608–616
[46] Varma SK, Kalyanam J, Murk LE, Srinivas V (1994) Effect of grain size on deformation-induced martensite formation in 304 and 316 stainless steels during room temperature tensile testing. J Mater Sci Lett 13:107–111
[47] Jung Y-S, Lee Y-K, Matlock DK, Mataya MC (2011) Effect of grain size on strain-induced martensitic transformation start temperature in an ultrafine grained metastable austenitic steel. Met Mater-Int 17:553
[48] Lee C-Y, Yoo C-S, Kermanpur A, Lee Y-K (2014) The effects of multi-cyclic thermo-mechanical treatment on the grain refinement and tensile properties of a metastable austenitic steel. J Alloy Compd 583:357–360
[49] Shrinivas V, Varma SK, Murr LE (1995) Deformation-induced martensitic characteristics in 304 and 316 stainless steels during room-temperature rolling. Metall Mater Trans A 26:661–671
[50] Sohrabi MJ, Mirzadeh H, Sadeghpour S, Mahmudi R (2023) Grain size dependent mechanical behavior and TRIP effect in a metastable austenitic stainless steel. Int J Plast 160:103502
[51] Hecker SS, Stout MG, Staudhammer KP, Smith JL (1982) Effects of strain state and strain rate on deformation-induced transformation in 304 stainless steel: Part I. Magnetic measurements and mechanical behavior. Metall Trans A 13:619–626
[52] Murr LE, Staudhammer KP, Hecker SS (1982) Effects of strain state and strain rate on deformation-induced transformation in 304 stainless steel: Part II. Microstructural study. Metall Trans A 13:627–635
[53] Staudhammer KP, Murr LE, Hecker SS (1983) Nucleation and evolution of strain-induced martensitic (b.c.c.) embryos and substructure in stainless steel: a transmission electron microscope study. Acta Metall 31:267–274
[54] Talonen J, Hänninen H, Nenonen P, Pape G (2005) Effect of strain rate on the strain-induced $\gamma \rightarrow \alpha'$-martensite transformation and mechanical properties of austenitic stainless steels. Metall Mater Trans A 36:421–432
[55] Lo KH, Shek CH, Lai JKL (2009) Recent developments in stainless steels. Mater Sci Eng R-Rep 65:39–104
[56] Soleimani M, Kalhor A, Mirzadeh H (2020) Transformation-induced plasticity (TRIP) in advanced steels: a review. Mater Sci Eng A 795:140023
[57] Galindo-Nava EI, Rivera-Díaz-del-Castillo PEJ (2017) Understanding martensite and twin formation in austenitic steels: a model describing TRIP and TWIP effects. Acta Mater 128:120–134
[58] Naraghi R (2009) Martensitic transformation in austenitic stainless steels. Department of Materials Science and Engineering, Royal Institute of Technology, Stockholm